Clays and Clay Minerals, Vol. 52, No. 3, 357–374, 2004.

EFFECT OF THE TETRAHEDRAL CHARGE ON THE ORDER-DISORDER OF THE CATION DISTRIBUTION IN THE OCTAHEDRAL SHEET OF SMECTITES AND ILLITES BY COMPUTATIONAL METHODS

C. I. Sainz-Díaz[1,*], E. J. Palin[2], A. Hernández-Laguna[1] and M. T. Dove[2]

[1] Departamento de Ciencias de la Tierra y Química Ambiental, Estación Experimental del Zaidín (CSIC), C/ Profesor Albareda, 1, 18008 Granada, Spain

[2] Department of Earth Sciences, University of Cambridge, Downing Street, Cambridge CB2 3EQ, UK

Abstract—The order-disorder behavior of the isomorphous cation substitution of the octahedral sheet of phyllosilicates was investigated by Monte Carlo simulations based only on atomistic models in some three-species systems Al/Fe/Mg including a wide range of different octahedral compositions that can be relevant to clay compositions found in nature, especially for smectites and illites. In many cases, phase transitions do not occur, in that long-range order is not attained, but most systems exhibit short-range order at low temperature. The ordering of the octahedral cations is highly dependent on the cation composition. Variations in the tetrahedral charge (smectite *vs.* illite) produce slight differences in the cation distribution and the short-range and long-range order of octahedral cations do not change drastically. The average size of Fe clusters and the long-range order of Fe are not larger in illites than in smectites as previous reports concluded, but the proportion of Fe^{3+} cations non-clustered is higher in smectites than in illites. This behavior supports the experimental behavior of the Fe effect on the Al-NMR signal, which is lower in illites than in smectites.

Key Words—Cation Ordering, Clay Minerals, Illites, Monte Carlo Simulations, Smectites.

INTRODUCTION

Phyllosilicates are able to undergo a wide variety of cation substitutions to produce large numbers of different minerals. Many of the possible substitutions relate to the sheet of octahedrally-coordinated cations which is present in almost all phyllosilicates. These sheets can accommodate many different cations, with those most commonly found being Al^{3+}, Fe^{3+} and Mg^{2+}. In dioctahedral 2:1 phyllosilicates, isomorphous substitution of Al^{3+} by Mg^{2+} in the octahedral sheet or Si^{4+} by Al^{3+} in the tetrahedral sheet results in a net negative charge that is balanced by the presence of cations in the interlayer space. Experimental determination of the distribution of cations within the sheets is a complex problem, due to small crystal size and high disorder level of the layers in clay minerals.

The cation distribution for the octahedral sheet of phyllosilicates has been studied previously. Experiments on phyllosilicates have yielded many and varied results for the configuration of octahedral sheets, particularly in natural samples of 2:1 phyllosilicates. A non-random distribution of cations was found in the octahedral sheet of celadonites, where the Al^{3+} and Fe^{3+} tend to segregate from each other (Besson *et al.*, 1987). Drits *et al.* (1997) studied the cation distribution in celadonites, glauconites and Fe-illites by infrared (IR), Mössbauer and extended X-ray absorption fine structure (EXAFS) spectroscopies together with simulations by probabilistic methods, finding certain short-range ordering. Schroeder (1993) found, by means of ^{27}Al nuclear magnetic resonance (NMR), that Fe mixes with Al in illite-smectite (I-S) in shales with low Fe content but Fe segregates from Al in Fe-rich specimens. In some synthesized smectites, Grauby *et al.* (1991) found that Al^{3+} and Fe^{3+} tend to mix rather than to segregate. In montmorillonites, Vantelon *et al.* (2003) found random Fe distributions for samples with low Fe content and clustered Fe for samples with high Fe content by means of EXAFS and IR spectroscopies. Fourier transform infrared (FTIR) and ^{27}Al NMR spectroscopic studies and Reverse Monte Carlo (RMC) simulations on illite-smectite samples showed a short-range ordering in the octahedral cations with a tendency to be segregated for Fe^{3+} cations and to be dispersed for Mg^{2+} cations (Cuadros *et al.*, 1999; Sainz-Díaz *et al.*, 2001a). Therefore, these different results make it difficult to extract a definitive conclusion from experimental works.

Computer simulations can play a useful role in these studies. Monte Carlo (MC) simulations have been shown to be a powerful tool for the study of cation distribution and ordering in minerals. In previous papers, we have investigated the order-disorder behavior of the tetrahedral sheet (Al/Si) in muscovite (Palin *et al.*, 2001); the tetrahedral (Al/Si) and octahedral (Al/Mg) sheets in phengite (Palin *et al.*, 2003); and the octahedral sheet in illites and smectites, both with respect to two-species systems Al/Fe, Al/Mg, Fe/Mg and to some three-species systems Al/Fe/Mg (Sainz-Díaz *et al.*, 2003a, 2003b), reproducing the experimental behavior.

* E-mail address of corresponding author:
sainz@eez.csic.es
DOI: 10.1346/CCMN.2004.0520311

In the illite-smectite system there is a natural mineral transformation from smectite to illite. The understanding of the mechanism of this transformation can be important, because the I-S distribution can be a descriptor for the exploration of underground oil deposits. The stability of the clay barriers for toxic and nuclear waste disposal is closely related to this smectite–illite transformation, changing the cation exchange and water-swelling capacity, thereby increasing the risk of leaks in the barrier. Previous FTIR studies of the OH-group vibrations on I-S samples showed short-range order in the cation distribution of the octahedral sheet (Cuadros *et al.*, 1999). No significant difference in the cation ordering was observed between smectites and illites. However, a new, interesting approach was included by means of the ^{27}Al NMR investigations. This technique can measure total intensities from the octahedral Al of phyllosilicates. The paramagnetic character of Fe causes it to interact with the applied magnetic field and creates a field inhomogeneity that causes a signal loss of ^{27}Al NMR. This effect of the Fe occurs only within a short radius around the Fe atom and can give us interesting information about the neighborhood of these Fe cations in the octahedral sheet of these minerals. Hence the analysis of the ^{27}Al NMR signal intensity along with the octahedral Fe and Al content permits an evaluation of the distribution of Fe within the octahedral sheet of phyllosilicates (Schroeder, 1993). A linear relationship was found between the illite proportion in I-S samples and the ^{27}Al NMR intensity. This phenomenon was explained by the existence of an additional medium- or long-range segregation of Fe cations in the octahedral sheet of illites that decreases the Fe effect on the ^{27}Al NMR signal (Cuadros *et al.*, 1999; Sainz-Díaz *et al.*, 2001a).

In this work, we extend our sampling of Al/Fe/Mg compositions with compositions relevant to naturally occurring clay minerals, especially for illites and smectites, in order to investigate the effect of the tetrahedral charge on the cation ordering in these minerals.

METHOD

We have developed a consistent approach to simulation studies of cation ordering, which we have described in detail (Bosenick *et al.*, 2001; Warren *et al.*, 2001). The ordering interactions in the crystal lattice of the mineral are computed by means of interatomic potentials and lattice-energy relaxation methods. These interactions are then used in Monte Carlo simulations to study the ordering process.

Simulation cell

Several models of dioctahedral 2:1 phyllosilicates with different compositions were studied (Table 1). These compositions represent isomorphous substitution of cations in the octahedral sheet and the octahedral vacancies are not involved in the cation substitution. All samples are dry and no interlayer water is included in the model. A unit-cell of smectite was previously (Sainz-Díaz *et al.*, 2001b) optimized using the program GULP (Gale, 1997) allowing relaxation of volume from experimental geometry (Tsipursky and Drits, 1984). From this optimized unit-cell, a $2 \times 2 \times 1$ supercell was built with periodic boundary conditions. This supercell includes 164 atoms and 16 octahedral sites. All configurations of this supercell with different compositions and cation distributions were optimized, allowing the simultaneous relaxation of the atomic positions and the cell parameters. A series of 90 random configurations of cation distribution in the octahedral sheet were generated using a computer program (MCCLAY99) described previously by Cuadros *et al.* (1999). These random configurations along with six ordered configurations were included in each simulation series.

Previous theoretical and experimental studies on micas with low tetrahedral Al content found a homogeneous distribution of the cations in the tetrahedral sheet with the Loewenstein rule of AlAl pair avoidance (Herrero and Sanz, 1991; Warren *et al.*, 2001). This homogeneous distribution was also included in this work by imposing partial occupancies of Si and Al in the crystallographic positions of the tetrahedral sheet according their compositions (Winkler *et al.*, 2002).

Interatomic potential model

The basic interatomic potential model (Table 2) was described previously elsewhere and was used to reproduce accurately structures and crystal properties of layered 2:1 phyllosilicates, especially smectites and illites (Sainz-Díaz *et al.*, 2001b).

Table 1. Chemical composition of the samples studied. Structural formulae on the unit-cell basis for $O_{20}(OH)_4$.

Sample	Si^{4+}	Al^{3+} (T)[a]	Al^{3+} (Oc)[a]	Mg^{2+}	Fe^{3+}	IC[a]
1	7.72	0.28	3	1		$K_{1.28}$
2	7.72	0.28	3	1		$Na_{1.28}$
3	7.2	0.8	3	1		$K_{1.8}$
4	7.72	0.28	3		1	$K_{0.28}$
5	7.2	0.8	3		1	$K_{0.8}$

[a] T: tetrahedral, Oc: octahedral, IC: interlayer cation

https://doi.org/10.1346/CCMN.2004.0520311 Published online by Cambridge University Press

Table 2. Parameters of the potential set model used in this work.

Short-range interactions [a]	A (eV)	ρ (Å)	C (eV Å^{-6})	Ref.
$Si^{4+}-O^{2-}$	1283.9073	0.3205	10.6616	b
$Si^{4+}-O^{1.426-}$	999.98	0.3012	0.0	b
$Al^{3+}-O^{1.426-}$	1142.6775	0.2991	0.0	c
$Al^{3+}-O^{2-}$	1460.3	0.2991	0.0	b
$Fe^{3+}-O^{2-}$ [d]	3219.335	0.2641	0.0	e
$Mg^{2+}-O^{1.426-}$	1142.6775	0.2945	0.0	b
$Mg^{2+}-O^{2-}$	1428.5	0.2945	0.0	b
$K^{+}-O^{2-}$	65269.71	0.2130	0.0	b
$Na^{+}-O^{2-}$	1271.504	0.3000	0.0	e
$O^{2-}-O^{2-}$	22764.0	0.149	27.88	b
$H^{0.426+}-O^{2-}$	325.0	0.25	0.0	b
Short-range interactions [f]	D (eV)	a (Å^{-1})	μ (Å)	
$H^{0.426+}-O^{1.426-}$	7.0525	2.1986	0.9485	b
Shell-core interaction	K (eV Å^{-2})	q_{core}	q_{shell}	
$O_{core}-O_{shell}$	74.92	+0.84819	−2.84819	b
Three-body bond-bending [g]	k (eVrad^{-2})	θ_o (°)		
$O^{2-}-Si^{4+}-O^{2-}$	2.09724	109.47		b
$O^{2-}-Al^{3+}(T)-O^{2-}$	2.09724	109.47		b
$O^{2-}-M(Oc)-O^{2-}$	2.09724	90		b
$O^{2-}-M(Oc)-O^{1.426-}$	2.09724	90		
$O^{1.426-}-M(Oc)-O^{1.426-}$	2.09724	90		

[a] Parameters for the Buckingham potentials between cation cores and oxygen shells. When the parameter C = 0.0, the function takes the form of Born-Mayer potentials. Cut-off at 12 Å
[b] Winkler *et al*. (1991)
[c] Schröder *et al*. (1992)
[d] with O^{2-}_{shell} or $O^{1.426-}_{core}$
[e] Bush *et al*. (1994)
[f] Modified Morse potential between cores
[g] T: in the tetrahedral sheet, Oc: in octahedral co-ordination
M: any cation in the octahedral sheet, Al^{3+}, Fe^{3+} and Mg^{2+}

Electrostatic Coulomb interactions are evaluated by the Ewald method using formal charges on all atoms, except for the OH species whose component atoms have partial charges chosen so as to reproduce the dipole moment of the OH group. The short-range cation/oxygen non-coulombic interactions are described by Buckingham potentials

$$E = A\exp(-r/\rho) - Cr^{-6} \quad (1)$$

where the exponential and the r^{-6} terms describe the repulsive energy and the longer range attraction, respectively. Covalent effects are simulated using three-body bond-bending interactions [$E = \frac{1}{2}k(\theta - \theta_0)^2$], where k is the harmonic three-body force constant, and θ and θ_0 are the observed and ideal bond angles, respectively. Values for the parameters A, ρ, C, k, and θ_0 are given in Table 2.

In the modeling of all oxygen atoms, except those from hydroxyl groups, electronic polarizability effects are taken into account by using the shell model. In this model the atoms are considered as a core comprising the nucleus and tightly bound inner electrons, surrounded by a massless shell of the remaining outer electrons. The core is assigned a charge of +0.84819e and the shell a charge of −2.84819e, maintaining the formal value for the overall ionic charge (Winkler *et al*., 1991). The shell and core are held together by an ideal harmonic core-shell interaction, $E = \frac{1}{2}K_s x_s^2$, where K_s is the harmonic force constant and x_s is the separation between the centres of core and shell. The O and H atoms within the hydroxyl group are given non-formal charge values, although the overall charge on the hydroxyl molecular ion has a formal charge of −1e. The interaction between these atoms is described by a Morse potential

$$E = D\{1 - \exp[-a(r - \mu)]\} \quad (2)$$

where r and μ are the observed and equilibrium interatomic distances, respectively. Values for the parameters D and a are given in Table 2. Coulomb forces are not included between atoms coupled by a Morse potential, as it is assumed that this potential describes all components of the interactions between both atoms.

https://doi.org/10.1346/CCMN.2004.0520311 Published online by Cambridge University Press

All lattice-energy calculations were performed by means of the GULP code with the Newton-Raphson minimization method for the lattice relaxation (Gale, 1997).

Determination of exchange interactions

The energy related to the ordering interactions can be extracted from the above lattice-energy calculations for the various configurations. Different relative positions between the octahedral sites can be defined in a two dimensional model as first, second, third and fourth nearest neighbors, according to the shortest different interatomic distances in the crystal (Figure 1). Considering the radial distribution function in this two-dimensional model, the intercationic distances can be classified in different ranges: <3.3, 5.1–5.3, 5.8–6.2, and 7.7–8.2 Å, defining the first, second, third and fourth neighbors, respectively. First of all, we consider a two-species system. The approach makes use of a Hamiltonian model for the ordering interactions. Taking into account separate pair interactions for two ordering cations (*A* and *B*), the energy of each configuration can be expressed as

$$H = E_0 + \sum_n (N^n_{A-A}E^n_{A-A} + N^n_{B-B}E^n_{B-B} + N^n_{A-B}E^n_{A-B}) \quad (3)$$

where n indicates the number of different types of neighboring pairs of cations, N is the number of cation pairs for each type, E is the partial energy related with this cation pairing, A and B can be Al^{3+}, Mg^{2+}, or Fe^{3+}, and the total energy requires summation over all types of interactions. E_0 is a constant that indicates all other components of bond energies and any energy that has no effect on the ordering process.

The separate energy terms for each neighbor pair can be combined into a single term called the exchange parameter (J). This parameter indicates the energy associated with the exchange of two cations to form $A-A$ and $B-B$ linkages instead of two $A-B$ linkages. Then, this energy expression can be reduced to

$$E = E_0 + \sum_n N^n_{A-A}J_n \quad (4)$$

where $J_n = E^n_{A-A} + E^n_{B-B} - 2E^n_{A-B}$, N^n_{A-A} is the number of $A-A$ interactions over a distance corresponding to a particular J_n, and E_0 is a constant term which is not involved in the ordering process. There are no terms dependent on B atoms, since these are wholly determined by those dependent on A atoms.

To proceed with the statistical analysis of the energies, it is useful to define an ordering variable (σ) for each site. We take the value $\sigma = -1$ if the site is occupied by A and $\sigma = +1$ if the site is occupied by B. Then, we can express the energy in terms of the following Hamiltonian model:

$$H = E_0 + \sum_n \sum_{<ij>} \sigma_i\sigma_j J_n \quad (5)$$

where <*ij*> shows that the sum is over all relevant pairs of octahedral sites, avoiding counting any pair twice. The Hamiltonian model holds for all values of the *A*:*B* ratios of the octahedral sheet (for our minerals, any Al:Mg, Al:Fe and Fe:Mg ratio). A more detailed discussion has been given elsewhere (Bosenick *et al.*, 2001). This model is particularly amenable for analysis by statistical mechanical tools such as the Monte Carlo method used in this work.

If similar analysis is performed for a system with A and C cations, and a system with B and C cations, then the J formalism can be extended to the case of three ordering species, A, B and C. Specifically, the pair energies for the two-cation systems are

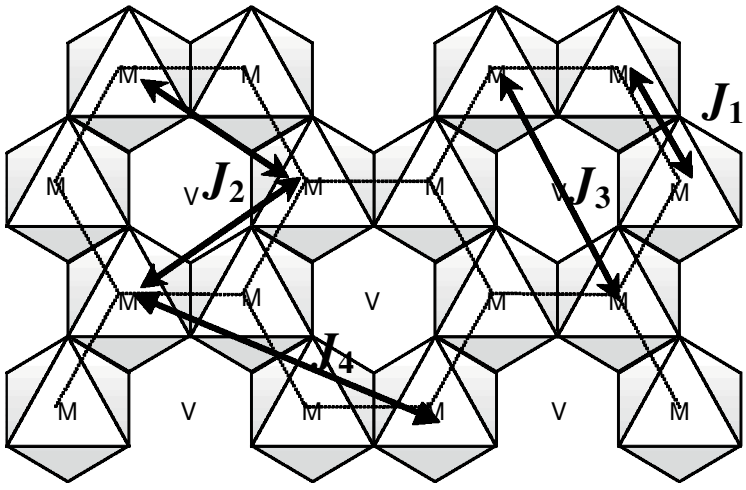

Figure 1. Exchange interactions between octahedral cations. M represents a filled octahedral site and V represents a vacant octahedral site.

https://doi.org/10.1346/CCMN.2004.0520311 Published online by Cambridge University Press

$$\begin{aligned} J^{AB} &= E_{A-A} + E_{B-B} - 2E_{A-B} \\ J^{AC} &= E_{A-A} + E_{C-C} - 2E_{A-C} \\ J^{BC} &= E_{B-B} + E_{C-C} - 2E_{B-C} \end{aligned} \quad (6)$$

It can be shown that for three cation types (Sainz-Díaz *et al*., 2003b), the energy becomes

$$E = E'_0 + \sum_n N^n_{A-A} J^n_{A-A} + N^n_{B-B} J^n_{B-B} + N^n_{C-C} J^n_{C-C} \quad (7)$$

where E'_0 is another constant term, different from E_0 in equation 1, and the J values (J^n_{A-A}, *etc*.) are given as a function of the J's from the two-cation systems:

$$\begin{aligned} J^n_{A-A} &= \tfrac{1}{2}[J^{(AB)}_n + J^{(AC)}_n - J^{(BC)}_n] \\ J^n_{B-B} &= \tfrac{1}{2}[J^{(AB)}_n + J^{(BC)}_n - J^{(AC)}_n] \\ J^n_{C-C} &= \tfrac{1}{2}[J^{(AC)}_n + J^{(BC)}_n - J^{(AB)}_n] \end{aligned} \quad (8)$$

where the $J^{(AB)}$, *etc*. are given in equation 6. Hence, with J values for the systems Al/Fe, Al/Mg, Fe/Mg, we can calculate values for the three-species system Al/Fe/Mg (Table 2).

The energy minimization of the different configurations generated provides 90 different lattice energies, which form a set of values for E in equation 4. For each configuration, all AB cation pairs (A or B = Al^{3+}, Mg^{2+} and Fe^{3+}) as first, second, third and fourth nearest neighbors were calculated with our MCCLAY99 program (Cuadros *et al*., 1999). The energies and the number of A–A cation interactions of each exchange pair for each configuration calculated by our program generated 90 equations of the form of equation 4 with the values of E_0 and exchange interactions to be determined by multiple regression analysis. Then, the different J_n exchange interactions of the two-cation systems are determined, and from these values the exchange interactions for the three-cation systems can be deduced.

Monte Carlo simulations

We performed Monte Carlo simulations for statistical analysis of the Hamiltonian of equation 4 by means of our own parallelized Ossia code (Warren *et al*., 2001). This MC simulation program yields information about the topology of the bonds between sites. The configuration is defined in terms of a lattice of unit-cells, as in a crystal, including periodic boundary conditions. Each unit-cell contains a set of labeled cation sites. Each configuration is defined by the set of cation pairs as first, second, third and fourth neighbors and by the energy (E) of equation 4. Supercells of $18 \times 18 \times 1$ were used for the simulations, *i.e*. 1296 cation sites on a single octahedral sheet. The starting configuration for the MC simulation can be random or with an ordered distribution. In this configuration, two cations are selected randomly and their positions are exchanged if this action lowers the Hamiltonian value, H, of equation 5. If H increases, the cation positions are exchanged with a probability $\exp(-\Delta H/T)$, where T is not an absolute temperature but a relative value of temperature. This step is repeated 10^6–10^8 times. In a first period, H decreases until the system reaches equilibrium. Then, H oscillates slightly around the minimum value and all data and average values are taken in this period. This procedure was repeated at different values of T (typically between 20 and 60 values of T), following a warming or a cooling process in order to avoid false minimum states in an annealing simulation process, with a total of 200 million equilibration steps per temperature. In some cases, subsequent simulations were run over smaller temperature ranges to examine the behavior near possible phase transitions.

At the end of each simulation, the thermodynamic quantities $\langle E \rangle$ and $\langle E^2 \rangle$ are output, from which the heat capacity C at constant pressure of the system can be calculated (Warren *et al*., 2001):

$$C = \frac{\langle E^2 \rangle - \langle E \rangle^2}{k_B T^2} \quad (9)$$

In the case of a second-order phase transition, the heat capacity will diverge at T_c and hence is a useful measure of any ordering phase transitions which may occur. It is especially useful for us in these simulations, since it is difficult to study phase transitions using order parameters when the ordering schemes observed can be very complicated.

The difference between long-range and short-range ordering is merely qualitative. There is no limit line between these orderings (Warren *et al*., 2001). A long-range order covers the whole ensemble, whereas short-range order covers order over a limited length scale and gives local fluctuations from the long-range order. The long-range order can be zero, because the average over the whole ensemble is zero, but correlations over short distances could be different from what would be obtained if all sites behaved as the average.

RESULTS

Several Al/Fe/Mg mixtures have been studied representing different octahedral cation compositions of 2:1 phyllosilicates. Previously, we studied different Al/Fe/Mg compositions corresponding to natural and synthetic phyllosilicates, covering a wide range of compositions from montmorillonites to nontronites and celadonites (Sainz-Díaz *et al*., 2003b; Palin *et al*., 2004). In this work, the investigation is centered on natural smectites and illite groups taking into account the tetrahedral charge effect on the octahedral cation ordering. In these samples the content of octahedral Al is always >50% and Fe^{3+} and Mg^{2+} comprise the remainder of the sites. Therefore, the following samples were investigated with respect to the Al/Fe/Mg relative proportion that for a set

https://doi.org/10.1346/CCMN.2004.0520311 Published online by Cambridge University Press

Table 3. Exchange interaction values (J_n) determined for two-species systems (in eV, values in brackets represent the standard error in the last figure).

Parameter	E_0	J_1	J_2	J_3	J_4
Distance (Å)	–	<3.3	5.1–5.3	5.8–6.2	7.7–8.2
Model 1 (AlMg)	−5300.45 (66)	0.656 (16)	0.168 (14)	0.089 (18)	0.025 (8)
Model 2 (AlMg)	−5299.42 (61)	0.652 (14)	0.162 (10)	0.088 (10)	0.015 (9)
Model 3 (AlMg)	−5222.25 (71)	0.620 (18)	0.151 (11)	0.066 (12)	0.030 (9)
Model 4 (AlFe)	−5376.14 (8)	0.025 (2)	0.007 (1)	0.003 (1)	0.003 (1)
Model 5 (AlFe)	−5292.83 (15)	0.015 (3)	0.005 (2)	0.008 (3)	0.001 (2)
Model 6 (FeMg)	−5211.68 (57)	0.456 (31)	0.101 (23)	−0.003 (27)	0.075 (20)

of six unit-cells (24 octahedral cations) will be: 16/4/4, 18/2/4, 16/2/6, 14/4/6, 14/8/2, 12/7/5, 12/8/4, 12/4/8 and 12/6/6. We have also included the Al/Fe/Mg = 8/8/8 sample, reported previously (Sainz-Díaz *et al.*, 2003b), since it has no composition preference of any cation and it can be a good initial reference for comparison purposes. Although some of these compositions are not normalized to the minimal proportion, we will maintain these proportions (for 24 cations) for a better comparison between all samples.

For each composition discussed in detail below, the lowest-energy configuration is given, since this is statistically the structure that will be the most ordered. For some of the lowest-energy configurations, plots are also shown of the individual Al, Fe and Mg cation networks. In these figures, Al and Fe atoms are linked together over J_1 distances, and Mg over J_3 distances. We will refer to these figures as 'partial ordering patterns'. Of particular interest are the Fe partial ordering patterns, in which only nearest-neighbor Fe–Fe linkages are shown, thereby enabling us to establish the size, shape and approximate number of Fe clusters present.

We also present data for the heat capacity in each system. We have determined that even for systems without perfect long-range order, there are often anomalies in the heat capacity at a certain temperature, and that sharper anomalies tend to correspond to better ordering. In our simulations, we compute at each temperature the number of linkages of each type (J_1, J_2, *etc.*) for each type of atom (Al, Fe, Mg). Plots of these parameters, $nJ_{n,i-i}$, as a function of temperature are sometimes useful in examining ordering processes.

Exchange interactions

The exchange interactions obtained from the calculations of all configurations and the Hamiltonian model (equation 4) of the two-species systems are described in Table 3 (Sainz-Díaz *et al.*, 2003a, 2003b). We derived values for interactions for the three-cation systems using these two-atom exchange interactions according to equation 8. Taking into account that the two-species exchange interactions have been obtained from samples of different composition in the tetrahedral sheet, different series of three-cation exchange interactions can be selected (Table 4): (a) averaged values derived from the mean of the two-atom exchange interactions (values from samples 1–3 for the Al/Mg systems, values from samples 4 and 5 for Al/Fe systems, and values from 6 for Fe/Mg mixture). This is reasonable since the MC simulations for two species displayed similar behavior in samples 1–3, and samples 4 and 5 showed similar behavior in the Al/Fe 1/1 system (Sainz-Díaz *et al.*, 2003a). (b) Smectite series, that are values derived from the two-atom exchange interactions of samples with low interlayer charge, like sample 1 for the Al/Mg system, sample 4 for the Al/Fe mixture, and sample 6 for Fe/Mg. (c) Illite series, derived from samples with higher interlayer charge, like sample 3 for the the Al/Mg system, sample 5 for the Al/Fe mixture, and sample 6 for Fe/Mg.

Al/Fe/Mg = 8/8/8

Dioctahedral phyllosilicates of the celadonite group can have approximately this composition in the octahedral sheet. This sample is the simplest three-species composition and corresponds to a minimal Al/Fe/Mg

Table 4. Exchange interactions for three-species systems (in eV), derived from those obtained for two-species systems (Table 3)[a].

Parameter	J_1	J_2	J_3	J_4
Al–Al	0.090[b], 0.113[c] (0.105)	0.028[b], 0.037[c] (0.033)	0.039[b], 0.048[c] (0.049)	−0.022[b], −0.024[c] (−0.029)
Fe–Fe	−0.075[b], −0.088[c] (−0.085)	−0.023[b], −0.030[c] (−0.027)	−0.031[b], −0.045[c] (−0.044)	0.023[b], 0.027[c] (0.031)
Mg–Mg	0.531[b], 0.544[c] (0.545)	0.124[b], 0.131[c] (0.127)	0.028[b], 0.042[c] (0.041)	0.052[b], 0.049[c] (0.049)

[a] Values in brackets are from averaged J values of two-species systems: Al/Mg values from samples 1–3, Al/Fe values from 4 and 5, and Fe/Mg values from 6. [b] Values from illites (3, 5 and 6). [c] Values from smectites (1, 4 and 6).

https://doi.org/10.1346/CCMN.2004.0520311 Published online by Cambridge University Press

composition of 1/1/1, reported previously (Sainz-Díaz *et al.*, 2003b). The averaged values set was used for the parameters of three-cation exchange interactions. The heat capacity anomaly (Figure 2a) shows a phase transition at approximately 580 K to produce an ordered structure (Figure 2b). The partial ordering pattern of Fe is represented in Figure 2c. The long-range and short-range order is almost perfect; only a few cations are erroneously placed.

The Mg and Al cations also exhibit long-range and short-range ordering. The Mg network is controlled mainly by J_2, J_3 and J_4 interactions forming ordered superstructures (Figure 2b). There are no MgMg nearest-neighbor pairs in the ordered configuration of this model, according to the experimental behavior of Mg^{2+} in the octahedral sheet of illites, smectites (Sainz-Díaz *et al.*, 2001a) and nontronites (Manceau *et al.*, 2000a). Besides, the Fe^{3+} cations segregate in small globular clusters, and this is consistent with the lack of magnetic ordering observed experimentally in nontronites at low temperatures (Lear and Stucki, 1990), where small Fe domains separated by Al and Mg cations were found (Manceau *et al.*, 2000a).

Samples with a medium amount of Al (50–60%)

In this group several samples can be included, Al/Fe/Mg = 12/4/8, 12/6/6, 12/7/5, 12/8/4, 14/8/2 and 14/4/6. These compositions can be found in natural and

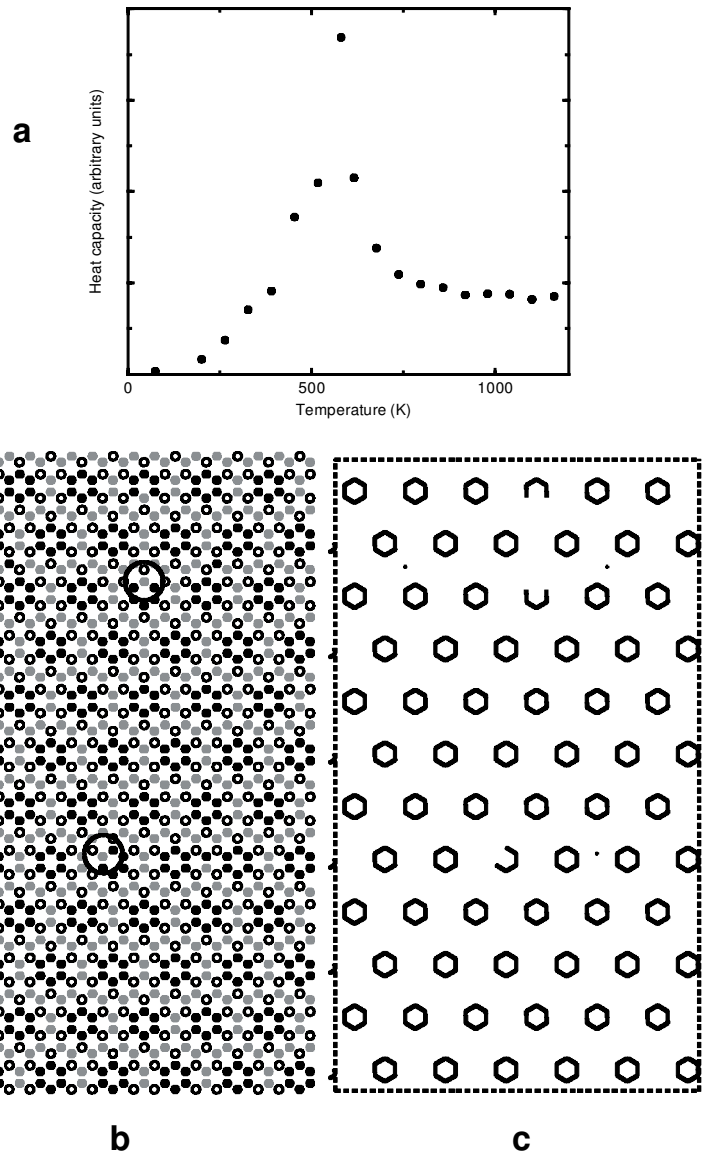

Figure 2. System Al/Fe/Mg = 8/8/8. (a) Variation of heat capacity with temperature. (b) Structural snapshot of the lowest-energy distribution at low temperature; gray circles indicating Al, black circles Fe and open circles Mg. Selected defects in the ordering pattern are ringed. (c) Partial ordering pattern for Fe cations only, showing J_1 linkages.

https://doi.org/10.1346/CCMN.2004.0520311 Published online by Cambridge University Press

synthetic smectites with high content of Fe^{3+} or Mg^{2+}, and with a unit-cell composition of $Al_2Fe_{0.67}Mg_{1.33}$, Al_2FeMg, $Al_2Fe_{1.17}Mg_{0.83}$, $Al_2Fe_{1.33}Mg_{0.67}$, $Al_{2.34}Fe_{1.33}Mg_{0.33}$, and $Al_{2.3}Fe_{0.7}Mg$, respectively.

The anomaly found in the heat-capacity profile with respect to the temperature is less sharp in these samples than in the previous sample (Figures 3a and 4a for Al/Fe/Mg = 12/4/8 and 12/8/4, respectively) but it is still clearly the ordering phase transition. This anomaly occurs at lower temperature in the samples with higher Fe content, and at a slightly lower temperature than in the previous sample Al/Fe/Mg = 8/8/8.

The lowest-energy distribution of the samples Al/Fe/Mg = 12/4/8 and 12/8/4 are shown in Figures 3b and 4b, respectively. For a better understanding, the partial ordering pattern of Fe was also included in Figure 4c. All samples of this group present similar ordering (Figures 3b, 4b and 5), and a lower degree of long-range order than in the previous sample Al/Fe/Mg = 8/8/8 was found. There is a fairly high degree of short-range order, but no significant long-range order. The Mg cations avoid J_1 linkages, forming a distribution controlled mainly by J_3 and also by J_2 and J_4 interactions. In contrast, the Fe atoms tend to cluster together to a certain

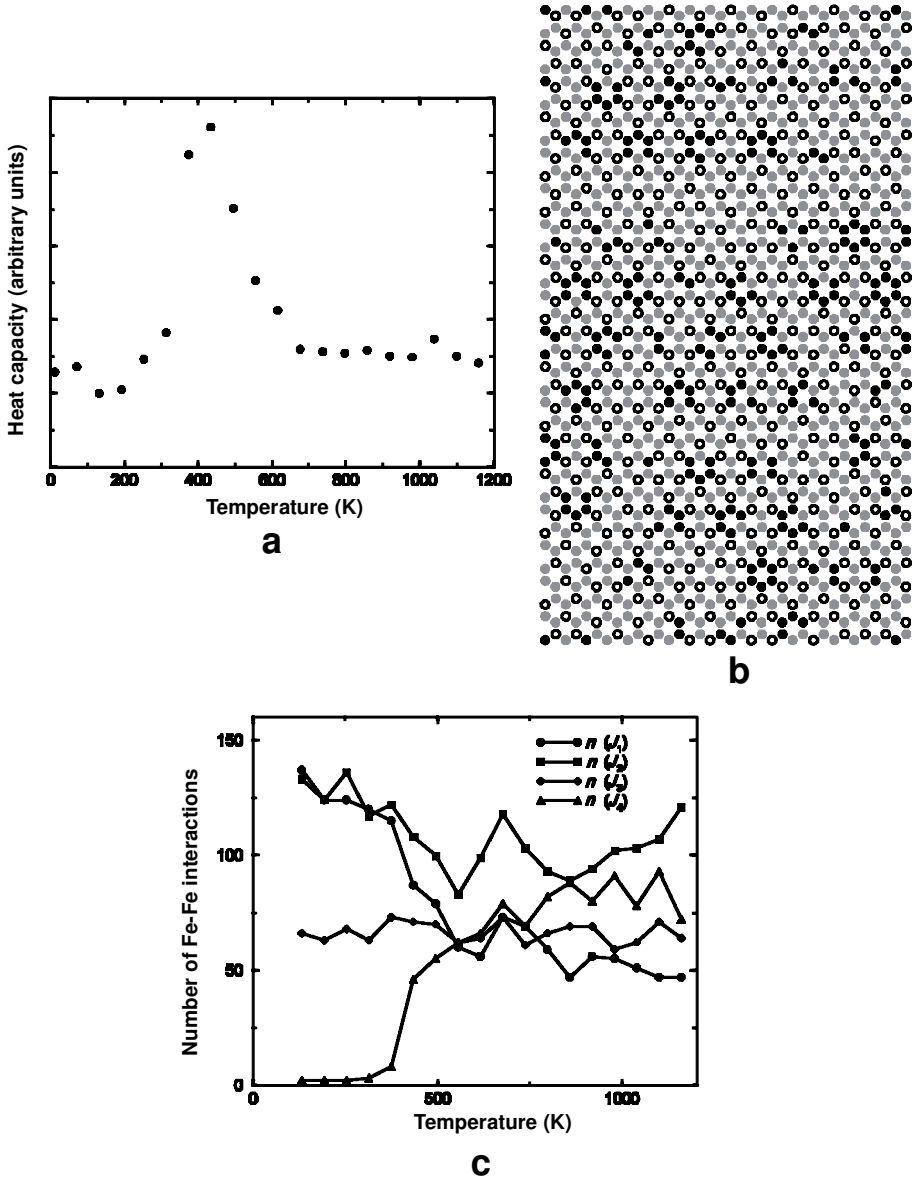

Figure 3. Heat capacity profile with temperature (a) for the system Al/Fe/Mg = 12/4/8. Snapshot of the lowest-energy structure at low temperature (b). Gray circles indicate Al, black circles Fe and open circles Mg. Plot of number of Fe–Fe interactions with temperature (c).

https://doi.org/10.1346/CCMN.2004.0520311 Published online by Cambridge University Press

extent. The clustering of the Fe atoms at low temperature can be observed from the $nJ_{n,\mathrm{Fe-Fe}}$ plot in Figure 3c. As the temperature decreases, the number of J_1 and J_2 linkages increases, while the number of J_4 linkages decreases. Hence, the Fe cations segregate in small clusters without long-range order.

The partial ordering pattern of Fe changes with the content of Fe and Mg in this group (Figures 3c, 4c and 5). Samples with high Mg and low Fe contents show that the Fe cations form clusters with a globular or pseudohexagonal shape (12/4/8 sample). However, in samples with higher Fe and lower Mg content, the Fe cations form clusters with a more linear shape (12/8/4 sample).

In the sample Al/Fe/Mg = 12/8/4, a certain long-range ordering is observed, with Fe atoms forming chains controlled mainly by J_1 and J_2 interactions (Figure 4c), and Al and Mg atoms segregating from Fe into different chains (Figure 4b). Cross-linking and inter-chain connections were not observed in the Fe chains. Perfect order was not attained in this system over the duration of our simulations. The Mg^{2+} cations are very dispersed in a MgMg network dominated by J_3 interactions with a small proportion of J_2 interactions. No specific ordering was found for Al^{3+} cations, being controlled mainly by J_1 and J_2 interactions. In this sample the long-range ordering for Fe, Mg and Al cations is higher than in the rest of the samples of this group

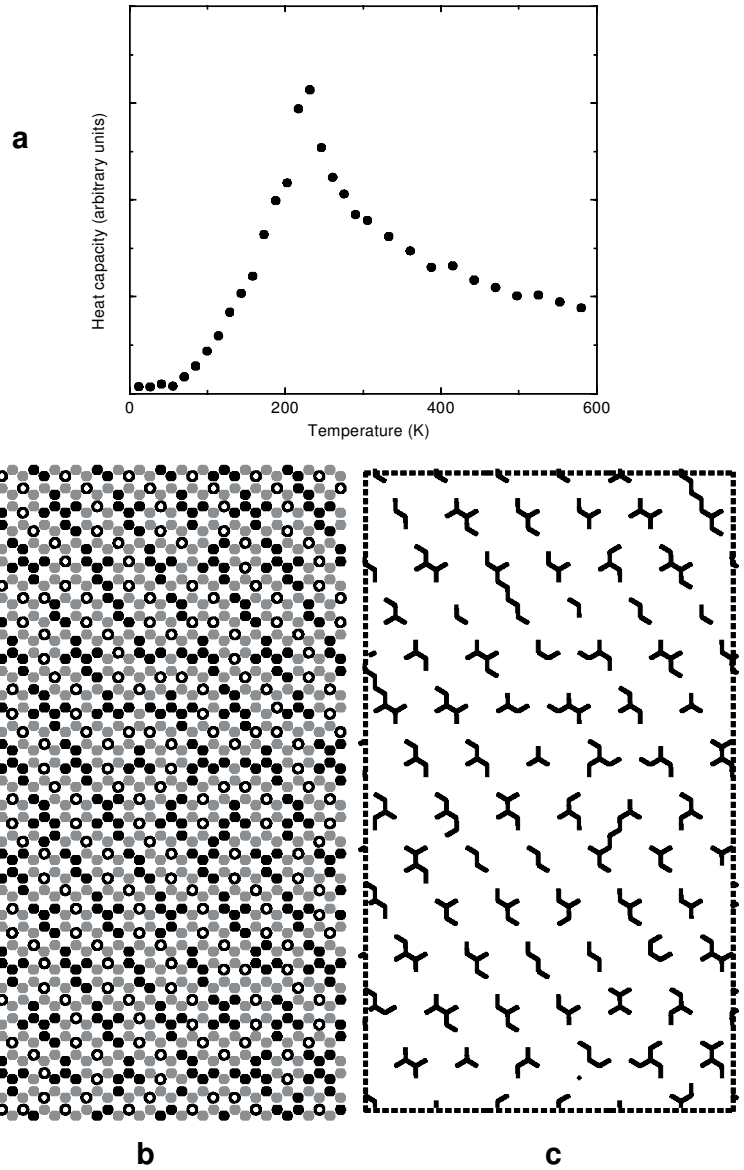

Figure 4. Plot of heat capacity as a function of temperature of the sample Al/Fe/Mg = 12/8/4 (a). Snapshot of the most stable structure (b). Gray circles indicate Al, black circles Fe and open circles Mg. Partial ordering pattern for Fe (c).

https://doi.org/10.1346/CCMN.2004.0520311 Published online by Cambridge University Press

Similar Mg arrangements were found experimentally in smectites (Sainz-Díaz *et al.*, 2001a) and nontronites (Manceau *et al.*, 2000a, 2000b). This segregation tendency of Fe^{3+} was also observed experimentally in natural smectites (Sainz-Díaz *et al.*, 2001a). However, this calculated long-range order was not observed in natural samples, where only short- and medium-length chains of Fe^{3+} were detected.

The sample Al/Fe/Mg = 14/4/6 represents an octahedral cation composition that can be found in natural smectites and illites (Cuadros *et al.*, 1999). Therefore, the three different sets of exchange interaction parameters J were used (averaged values, smectite set and illite set, Table 4), to perform three sets of simulations.

All simulation sets give similar results, and no significant difference between smectite and illite was

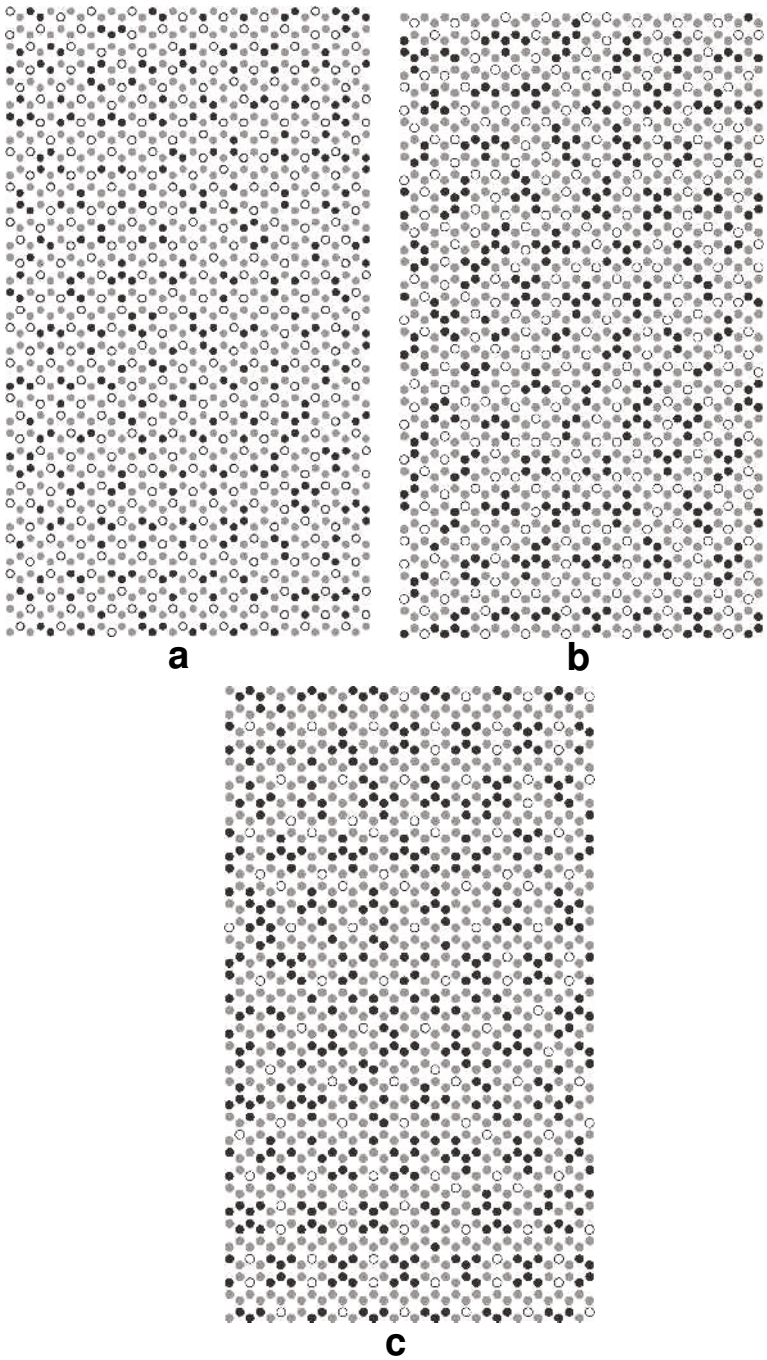

Figure 5. Lowest-energy cation distribution snapshots for the samples Al/Fe/Mg = 12/6/6 (a), 12/7/5 (b), 14/8/2 (c). Gray circles indicate Al, black circles Fe and open circles Mg.

https://doi.org/10.1346/CCMN.2004.0520311 Published online by Cambridge University Press

found. The most stable ordered configuration (Figure 6a,b) shows a highly dispersed Mg distribution dominated mainly by J_3 interactions, with J_2 and J_4 interactions also participating. The partial ordering pattern of Fe cations is shown in Figure 6c. The Fe cations show a certain short-range order segregating in very small clusters with no long-range ordering. The higher Mg content with respect to the sample 14/8/2 causes a lower long-range order of Fe. The Fe cluster size is similar for smectite and illite composition.

Samples with large amounts of Al (70–75%)

In this group several samples were selected: Al/Fe/Mg = 16/2/6, 16/4/4, 16/6/2, 18/2/4 and 18/4/2. These octahedral cation compositions can be found in natural illites and smectites (Cuadros *et al.*, 1999) with a unit-cell octahedral sheet formula $Al_{2.7}Fe_{0.3}Mg$, $Al_{2.7}Fe_{0.7}Mg_{0.7}$, $Al_{2.7}FeMg_{0.3}$, $Al_3Fe_{0.33}Mg_{0.67}$ and $Al_3Fe_{0.67}Mg_{0.33}$, respectively. Some natural montmorillonites also present similar octahedral composition, such as those from Georgia and Arizona (Vantelon *et al.*, 2003). Once again, therefore, three simulations were carried out with the three different sets of exchange interaction parameters J selected above (averaged values, smectite set and illite set, Table 4).

The most stable ordered configurations show similar ordering in all simulation sets and no significant difference between smectite (Figures 7a–11a) and illite

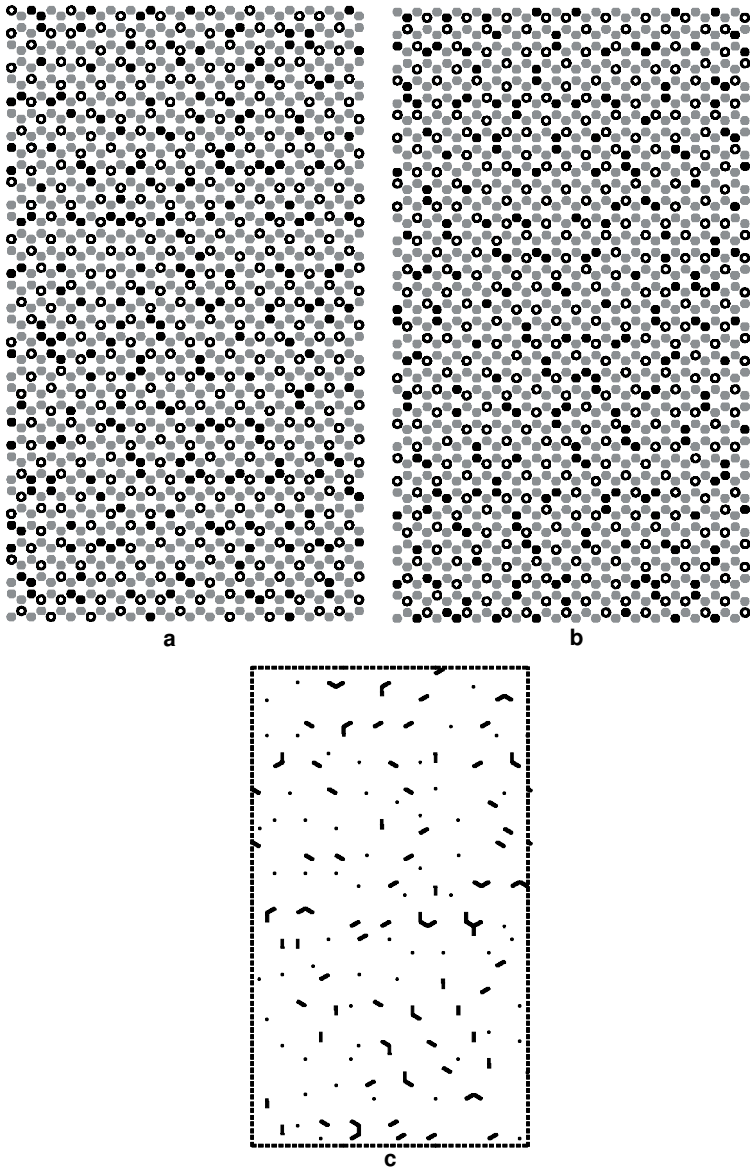

Figure 6. System Al/Fe/Mg = 14/4/6. Lowest-energy cation distribution snapshot for simulations performed with (a) smectitic and (b) illitic J values (see Table 4). Gray, black and white circles indicate Al, Fe and Mg, respectively. (c) Partial ordering pattern for Fe, showing J_1 linkages for a simulation performed with averaged J values (see Table 4).

https://doi.org/10.1346/CCMN.2004.0520311 Published online by Cambridge University Press

(Figures 7b–11b) was found, as in the former sample. In the most stable configuration, the Mg cations are again highly dispersed, with the distribution being dominated by J_3 and J_4 interactions with a long-range ordering similar to the former group. Ordered superstructures are observed for the Mg distribution in the samples 16/2/6 and 18/2/4, forming intercalated superhexagons with a Mg–Mg distance close to 6 Å (sample 16/2/6) or 9.1 Å (sample 18/2/4). The Fe cations are mostly isolated or paired, with J_1 and J_2 interactions dominant. In this group, the Fe content is too low for long-range ordering to occur. The high Mg content with respect to Fe inhibits the clustering of Fe in the sample 16/2/6, hence it is lower than in the former group. This behavior is due to the strong tendency of Mg to be dispersed (high J_1^{Mg-Mg} value).

Subtle differences can be observed between the simulations of smectite and illite sets (Figure 12). The systems a, b, c and d, e, f of Figure 12 represent the partial ordering pattern of Fe, Al and Mg in the most stable configuration for smectite and illite compositions, respectively. In the Al partial ordering patterns in this figure, Al atoms are connected only by J_1 linkages, rather than by both J_1 and J_2 linkages, for clarity. In the lowest-energy configuration of both systems, the Fe cations segregate forming small clusters of Fe, which are occasionally larger in the illite model (Figure 12d). The Mg network is dominated by J_3 interactions in all cases. However, the long-range order of Mg is slightly lower in smectites (Figure 12c) than in illites, where some linear distributions of Mg can be observed (Figure 12f). On the contrary, the Al partial ordering patterns show a slightly lower long-range ordering in illites (Figure 12e) than in smectites, which exhibit some linear distributions of Al (Figure 12b).

In general, no significant difference in the size of the Fe clusters was detected between the smectite and illite systems.

DISCUSSION

The results presented in this work show that the cation ordering is highly dependent on the relative cation composition in these three-species systems. Taking into account the most stable octahedral configuration of each of the samples presented above, Mg atoms are always dispersed with respect to each other. This is due to the high value of the J_1 and J_2 exchange interaction parameters for Mg–Mg, which are significantly higher than those for the Al–Al and Fe–Fe systems (Table 4). Thus, the occurrence of two Mg cations as nearest- or next-nearest-neighbors will be unfavorable, because this would contribute to significant increase of the energy of the system. This high value of the J exchange potentials can come from the larger ionic radius of Mg and the charge of the Mg^{2+} cation, that can produce an extra distortion when two Mg^{2+} cations are too close. In contrast, Fe cations tend to segregate, forming clusters with different size and shape depending on the octahedral composition of the sample. This behavior also has an energetic origin, due to the low and negative values of the J_1, J_2, and J_3 exchange potentials (Table 4). Thus, a segregation of Fe cations will produce a negative contribution to the total energy, thus

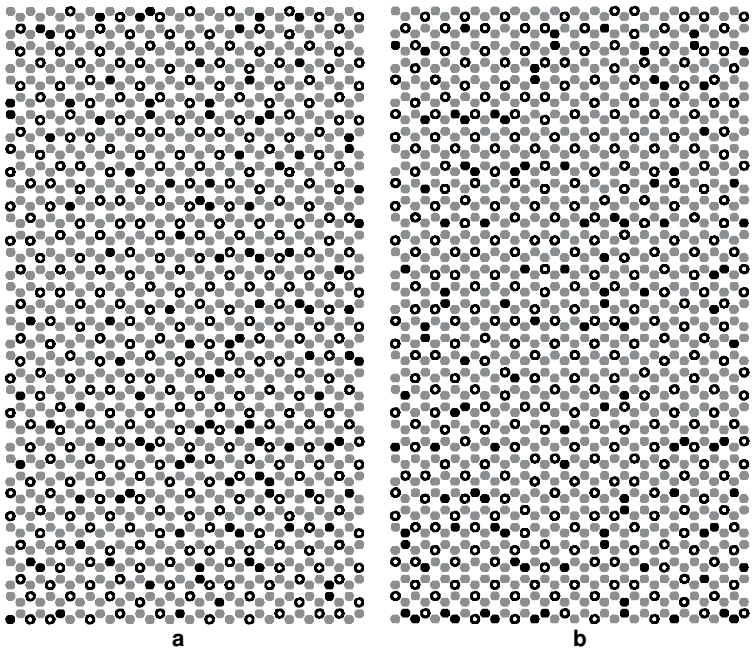

Figure 7. Lowest-energy cation distribution snapshots of Al/Fe/Mg = 16/2/6 system for smectite (a) and illite (b) composition (gray, black and white circles indicate Al, Fe and Mg, respectively).

https://doi.org/10.1346/CCMN.2004.0520311 Published online by Cambridge University Press

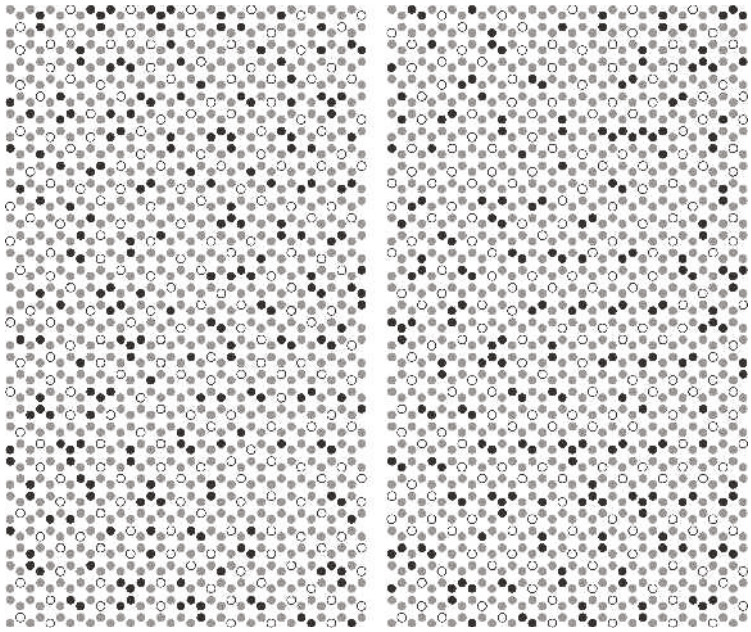

Figure 8. Snapshot of the lowest-energy structure at low temperature, Al/Fe/Mg = 16/4/4 system, for smectite (a) and illite (b) composition (gray, black and white circles indicate Al, Fe and Mg, respectively).

stabilizing the system. On the other hand, the behavior of Al atoms appears simply to adjust itself to accommodate the behavior of the Fe and Mg. This clustering behavior of Fe is also observed in experiments (Besson *et al*., 1987; Drits *et al*., 1997; Cuadros *et al*., 1999).

For I-S with low Al content and high Fe and Mg contents, the Fe cation forms globular clusters with no connectivity between clusters. Similar results were found recently in MC simulations on nontronites (Palin *et al*., 2004) although with a greater long-range ordering than in our samples. This result agrees also with experiment

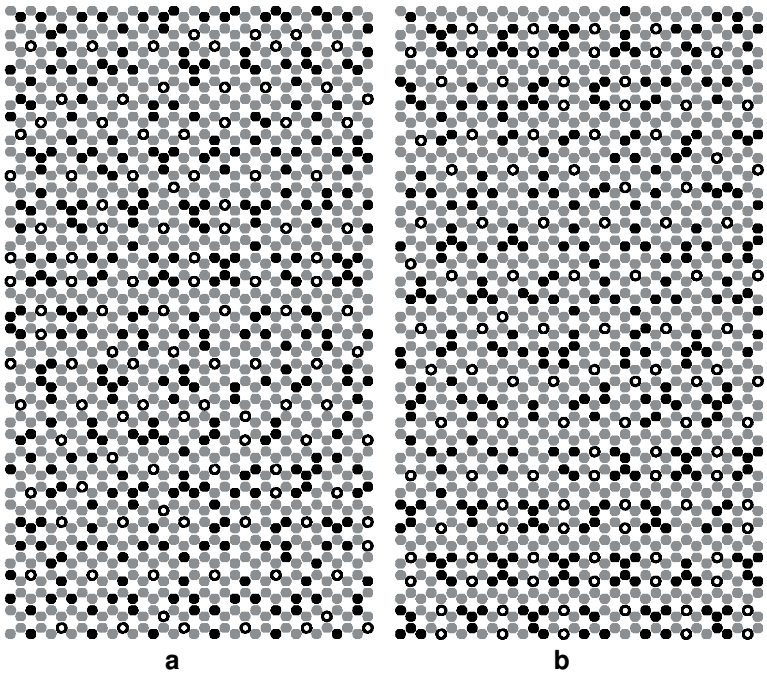

Figure 9. Lowest-energy cation distribution snapshots of sample Al/Fe/Mg = 16/6/2 for smectite (a) and illite (b) composition (gray, black and white circles indicate Al, Fe and Mg, respectively).

https://doi.org/10.1346/CCMN.2004.0520311 Published online by Cambridge University Press

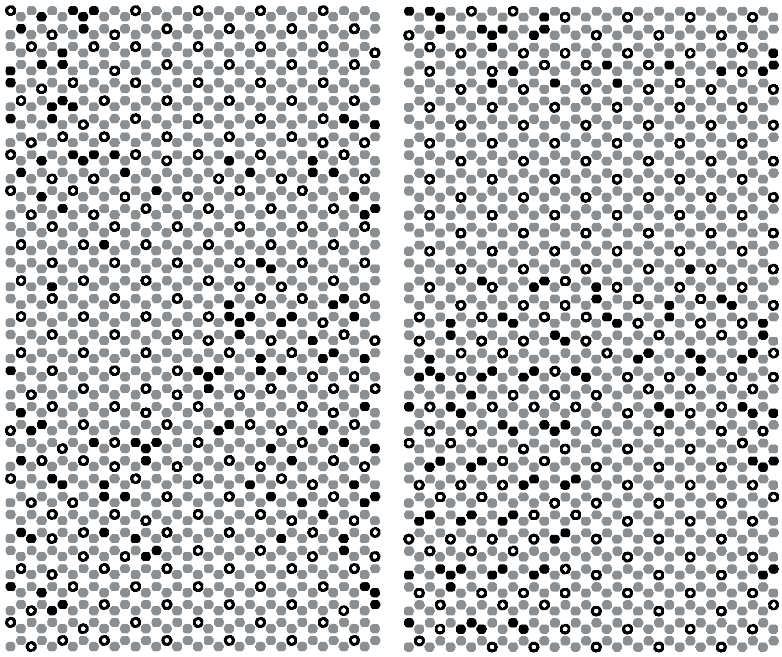

Figure 10. System Al/Fe/Mg = 18/2/4. Lowest-energy cation distribution snapshots for smectite (a) and illite (b) composition (gray, black and white circles indicate Al, Fe and Mg, respectively).

(Manceau *et al*., 2000a, 2000b), where small Fe domains separated by Al and Mg were found in nontronites. The lack of connections between Fe clusters is consistent with experimental results on nontronites by Lear and Stucki (1990), who showed that a lack of magnetic ordering was observed at low temperatures. In ferruginous smectites from Washington, Vantelon *et al*. (2003) also found a clustering of Fe^{3+} cations and dispersed Mg by means of IR and EXAFS spectroscopies. On the contrary, Manceau *et al*. (2000b) proposed a random distribution of Fe for

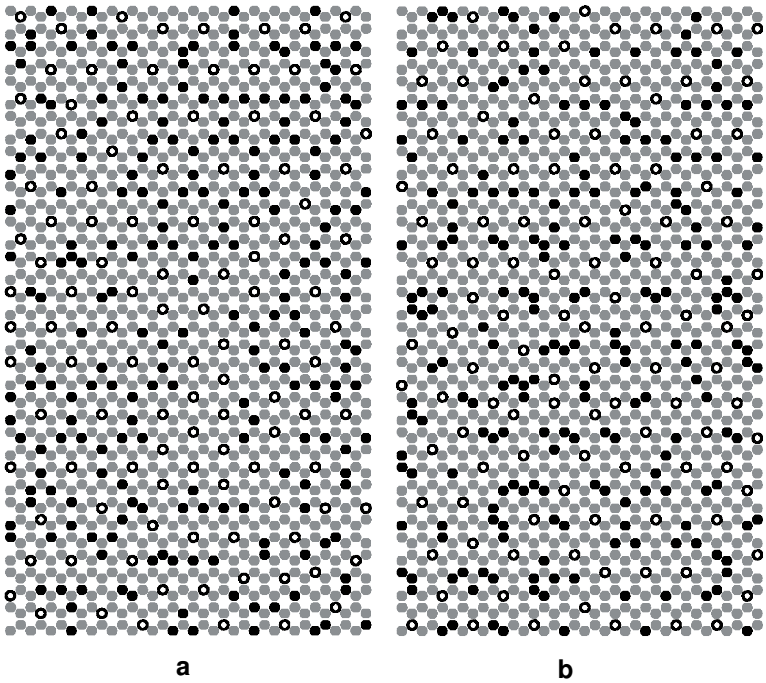

Figure 11. Snapshot of the lowest-energy structure at low temperature Al/Fe/Mg = 18/4/2 system for smectite (a) and illite (b) composition (gray, black and white circles indicate Al, Fe and Mg, respectively).

https://doi.org/10.1346/CCMN.2004.0520311 Published online by Cambridge University Press

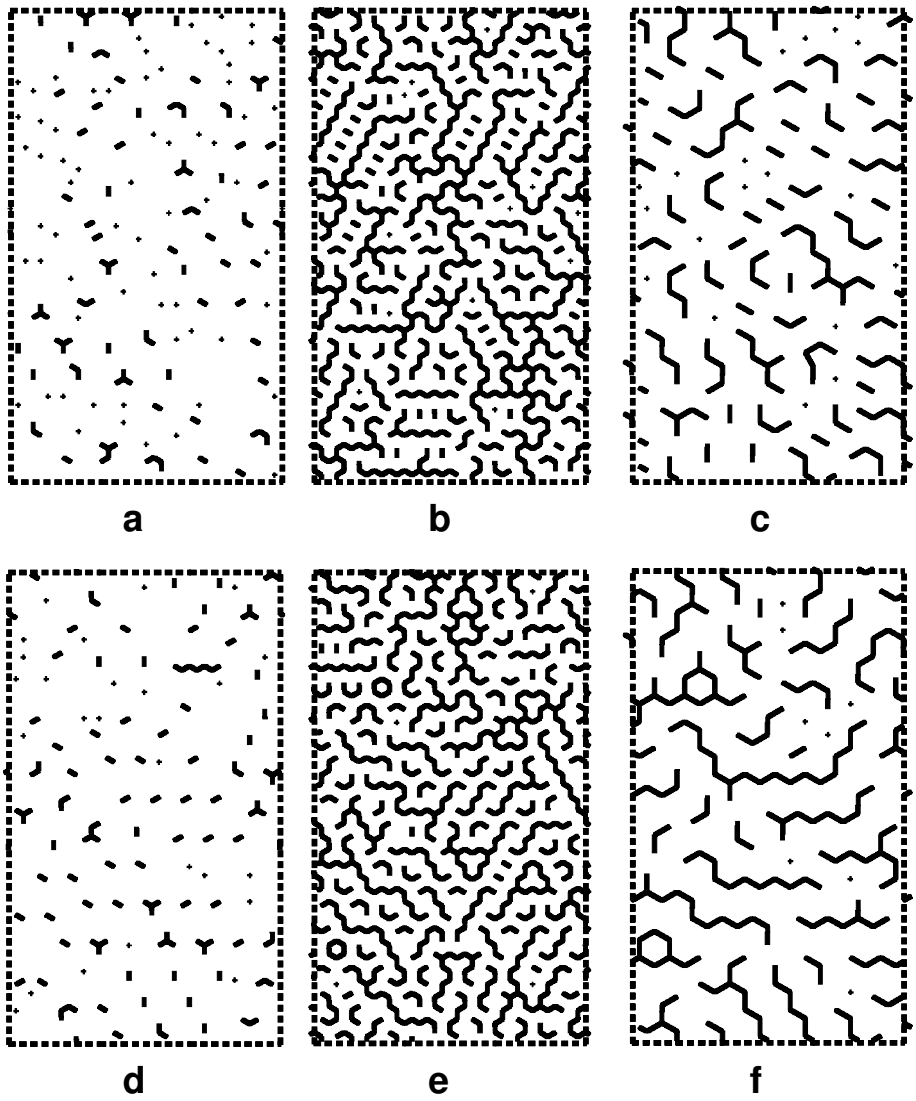

Figure 12. Partial-ordering pattern of the lowest-energy cation distribution of Fe (J_1 linkages), Al (J_1 linkages), and Mg (J_3 linkages) in Al/Fe/Mg = 16/4/4 with smectite composition (a, b and c, respectively) and illite composition (d, e and f, respectively).

this Washington smectite on the basis of polarized EXAFS experiments.

When the Al content increases to 50%, but with a greater Mg than Fe content, the long-range ordering decreases and the Fe clusters take different shapes (*e.g.* Al/Fe/Mg 12/4/8 sample). When the Fe content increases and is greater than the Mg content, the Fe clusters are linear with ramifications maintaining a certain long-range ordering (*e.g.* Al/Fe/Mg 12/8/4 and 14/8/2 samples).

In samples with very high Al content (>67%), as in many smectites and illites, Fe cations form only pairs or small clusters, without long-range ordering. The Mg cations can form superstructures with a certain degree of long-range ordering. This is consistent with previous experimental studies on illites and smectites (Cuadros *et al.*, 1999; Sainz-Díaz *et al.*, 2001a).

It should be noted that all these theoretical simulations correspond to the most stable octahedral cation configurations. All the long-range ordered configurations are ideal states controlled thermodynamically that may be found only rarely in nature. From the point of view of the natural formation process, the crystallization process could be too fast to yield a thermodynamically stable cation configuration, especially in mineral formation under hydrothermal conditions (dissolution-precipitation). In the diagenesis of smectites and illites, a kinetically very slow equilibration process of cation arrangements can probably occur, which favors the formation of a thermodynamically stable cation configuration. Therefore, it is possible to find short-range ordering in natural samples of smectites and illites.

This point is very interesting for the formation of synthetic dioctahedral 2:1 phyllosilicates, where the

https://doi.org/10.1346/CCMN.2004.0520311 Published online by Cambridge University Press

chemical compositions and kinetics can be controlled. For instance, special concentrations of cations could be explored in the synthesis of clays with magnetic properties looking for specific long-range ordering of Fe cations. Further research in this field can help to control the cation ordering during the formation of these synthetic clay minerals.

Ordering phase transitions

From this work, only the samples Al/Fe/Mg = 8/8/8 and 12/8/4 exhibit clear ordering phase transitions, where the heat-capacity profile with temperature has a sharp change. The ordered configuration of these samples has a long-range ordering at low temperature. The transition temperature of the sample 12/8/4 (Figure 4) is smaller than the 8/8/8 (Figure 2). The behavior of the 12/4/8 sample is rather more indistinct, although consideration of both the heat capacity profile and the lowest-energy structure suggests that it can be classified as a phase transition, especially in view of the sharp changes in the $n(J_{Fe-Fe})$ plot.

The rest of the samples do not present a clear ordering phase transition, but only a heat-capacity anomaly. These samples exhibit only short-range ordering at low temperature. Taking into account the heat capacity anomaly temperatures, a linear relationship between these temperatures and the Mg/Al ratio in octahedral composition is observed (Figure 13). For a similar Fe relative content, the higher the Mg content, the higher the transition temperature. The 12/8/4 sample exhibits a slightly lower transition temperature than this relationship, due to the higher content of Fe that decreases the transition temperature. This behavior is directly related to the relative values of the exchange interaction parameters J_i.

Effect of the tetrahedral charge – smectite vs. illite

Most of the samples studied in this work exhibit an octahedral composition that can be found in many natural smectites and illites. These minerals have similar octahedral compositions; the main difference between them is the tetrahedral charge, which is higher in illites than in smectites. Therefore, the application of these ordering MC simulations on samples with different tetrahedral charge could be interesting with respect to any potential changes in ordering.

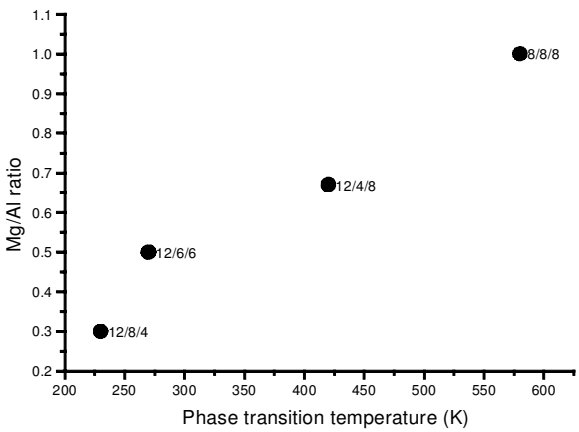

Figure 13. Plot of heat-capacity anomaly temperatures with the Mg/Al ratio in octahedral composition.

In all MC simulations presented above, we used three-species exchange interactions, J_i, values derived from averaged values of the two-species exchange interactions (Table 1). However, although the values in Table 1 are very similar for the same two-cation compositions (*e.g.* sets 1–3 for Al/Mg), we can distinguish two kinds of values: those obtained from samples with high tetrahedral charge ($Si_{7.2}Al_{0.8}$ by unit-cell) defining the illite model, and those obtained from samples with low tetrahedral charge ($Si_{7.72}Al_{0.28}$ by unit-cell) comprising the smectite model. Therefore, these three sets (averaged, smectites and illite models) were taken into account in those samples whose composition is very common in natural smectites and illites (samples 14/4/6, 16/2/6, 16/4/4, 16/6/2, 18/2/4 and 18/4/2).

Apparently no significant difference is observed between smectites and illites with the same composition. Only short-range ordering for Fe cations and very small Fe clusters (or Fe pairs) are found in both minerals. Nevertheless, in all samples, subtle differences can be observed. The Fe cluster size in illites is not larger than in smectites, as was thought previously; in fact, they are similar. However, the number of isolated Fe cations (non-clustered) is larger in smectites than in illites. Observing the radial distribution function (RDF) of Fe with respect to other Fe cations, a high cation density appears at 3 Å as first-neighbor distance in the octahedral sheet and the cation density drops drastically in all samples. This observation confirms the short-range ordering of Fe in small cluster size. However, the relative intensity of the peak at 3 Å with respect to the rest of the peaks is greater in illites than in smectites (Figure 14a,b). This means that the clustering level is higher in illites than in smectites. On the other hand, the intensity of the peak at 6 Å is greater in smectites than in illites. This is related to the more negative value of J_3 obtained in smectites than from illites (Table 4).

The RDF of Mg shows the high dispersion level of Mg cations along the octahedral sheet where no MgMg pair as first and second neighbors is detected in the 18/2/4 sample. In samples 16/2/6 and 14/4/6 a small proportion of Mg at 5.2 Å was detected. No significant difference in Mg RDF was observed between smectites and illites (Figure 14c,d). These RDF results match the RDF profiles obtained from experimental data (Sainz-Díaz *et al.*, 2001a) reproducing the I-S differences.

Previous experimental studies in clay minerals (Besson *et al.*, 1987; Drits *et al.*, 1997) found that the

https://doi.org/10.1346/CCMN.2004.0520311 Published online by Cambridge University Press

Fe distribution is not random and it tends to segregate from Al with some short-range ordering, but no clear description of this ordering was reported. The RMC simulations based only on FTIR spectroscopic data of interstratified I-S (Cuadros *et al.*, 1999) found the existence of Fe clusters in both systems with larger cluster sizes in illites than in smectites. The IR data give information about short-range ordering, but the degree of clustering can only be estimated. Further RMC simulations based simultaneously on FTIR and ^{27}Al NMR data of these minerals (Sainz-Díaz *et al.*, 2001a) corroborated the Fe clustering tendency, and the Fe clusters were actually very small and similar to those obtained in the present work. The RDF of Mg and Fe of the configurations obtained from these experimental data were similar to those obtained in the present work, and the inhibitor effect of the Fe on the Al NMR signal was higher in smectites than in illites. This experimental study could reproduce this effect but no clear justification could be reported. Besides, Fe-rich illites exhibited an extraordinarily strong Al NMR signal. These questions were explained by the possible existence of long-range order for Fe cations or a larger cluster size of Fe in illites than smectites (Sainz-Díaz *et al.*, 2001a).

CONCLUSIONS

Our MC simulations reproduce the cation distribution pattern of Fe^{3+} for illites and smectites found experimentally and clarify the previous tentative explanation (Sainz-Díaz *et al.*, 2001a). Illites do not exhibit long-range ordering of Fe and the Fe cluster size is not larger than in smectites. The decrease of inhibitor effect of Fe on the Al NMR signal with the illite proportion is due to the decrease of number of non-clustered Fe in illites. The good agreement between our simulations and the experiment can be related to the characteristics of the experimental samples. The experimental study of interstratified I-S samples (Cuadros and Altaner, 1998) found that bentonite samples are transformed from smectites to illite by means of a slow solid-state mechanism with no dissolution-precipitation-crystallization process. This mechanism allows for atom reorganization being slow enough to create a thermodynamically controlled process to yield the most stable cation distribution. Therefore, this smectite illitization would cause an increase in Fe segregation in the octahedral sheet. The control on our simulations is necessarily thermodynamic rather than kinetic, hence the good agreement between the two studies.

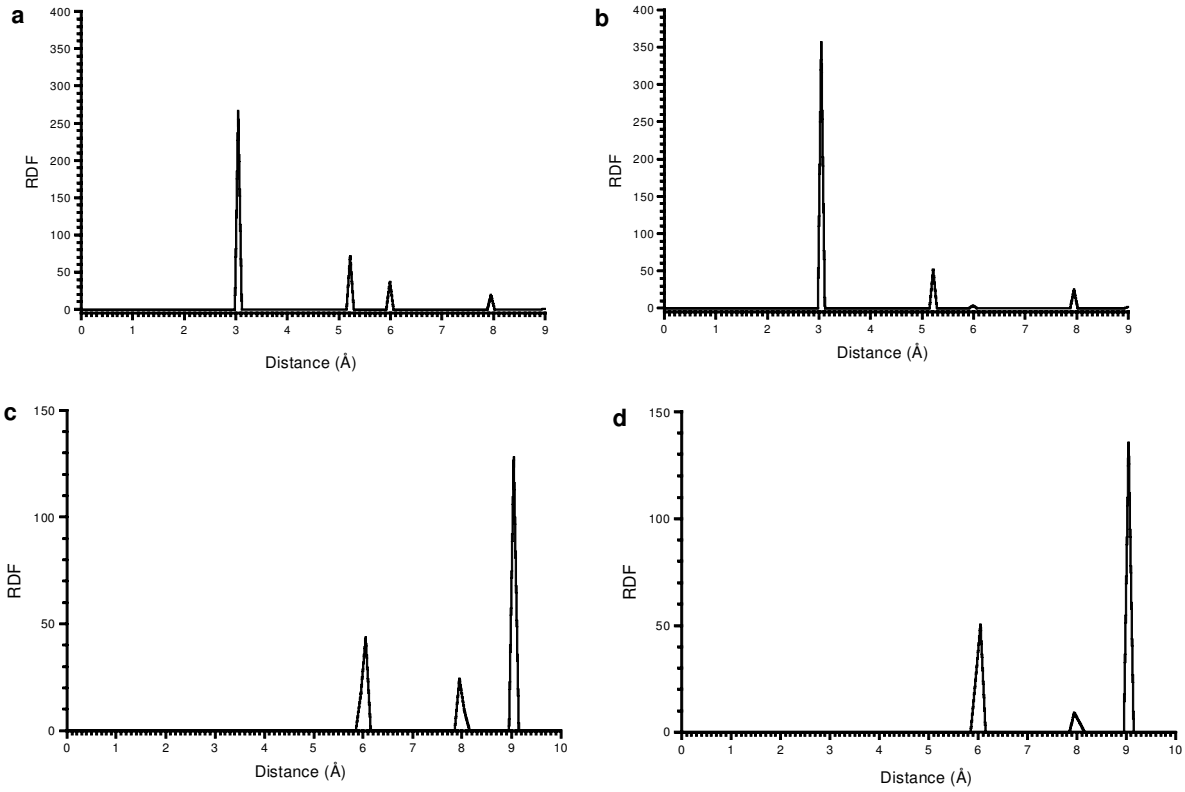

Figure 14. Radial distribution function (RDF) of Fe for Al/Fe/Mg = 18/2/4 with smectite (a) and illite (b) composition. RDF of Mg with smectite (c) and illite (d) composition.

https://doi.org/10.1346/CCMN.2004.0520311 Published online by Cambridge University Press

The good agreement with experiment found in this work validates this theoretical approach as a useful tool for experimentalists to predict cation ordering with respect to the cation composition in synthesis of clay minerals.

ACKNOWLEDGMENTS

The authors are grateful to R. Cygan for fruitful discussions, and to NERC (M.T. Dove), to EPSRC (E.J. Palin), to the exchange program of the Royal Society of the UK/CSIC of Spain (C.I. Sainz-Díaz), and to the BTE2002-03838 MCYT project (A. Hernández-Laguna) for financial support and to Centro Técnico de Informática of CSIC for the computing facilities. The Monte Carlo simulations were performed on the Mineral Physics Group's Beowulf cluster at the Department of Earth Sciences, University of Cambridge, and on the University of Cambridge's High Performance Computing Facility.

REFERENCES

Besson, G., Drits V.A., Dainyak, L.G. and Smoliar, B.B. (1987) Analysis of cation distribution in dioctahedral micaceous minerals on the basis of IR spectroscopy data. *Clay Minerals*, **22**, 465–478.

Bosenick, A., Dove, M.T., Myers, E.R., Palin, E.J., Sainz-Díaz, C.I., Guiton, B., Warren, M.C., Craig, M.S. and Redfern S.A.T. (2001) Computational methods for the study of energies of cation distributions: applications to cation-ordering phase transitions and solid solutions. *Mineralogical Magazine*, **65**, 193–219.

Bush, T.S., Gale, J.D., Catlow, C.R.A. and Battle, P.D. (1994) Self-consistent interatomic potentials for the simulation of binary and ternary oxides. *Journal of Material Chemistry*, **4**, 831–837.

Cuadros, J. and Altaner, S.P. (1998) Compositional and structural features of the octahedral sheet in mixed-layer illite/smectite from bentonites. *European Journal of Mineralogy*, **10**, 111–124.

Cuadros, J., Sainz-Díaz, C.I., Ramírez, R. and Hernández-Laguna, A. (1999) Analysis of Fe segregation in the octahedral sheet of bentonitic illite-smectite by means of FT-IR, ^{27}Al MAS NMR and reverse Monte Carlo simulations. *American Journal of Science*, **299**, 289–308.

Drits, V.A., Dainyak, L.G., Muller, F., Besson, G. and Manceau, A. (1997) Isomorphous cation distribution in celadonites, glauconites and Fe-illites determined by infrared, Mössbauer and EXAFS spectroscopies. *Clay Minerals*, **32**, 153–179.

Gale, J.D. (1997) GULP: a computer program for the symmetry-adapted simulation of solids. *Journal of Chemical Society, Faraday Transactions*, **93**, 629–637.

Grauby, O., Petit, S. and Decarreau, A. (1991) Distribution of Al-Fe-Mg in octahedral sheets of synthetic smectites: Study of three binary solid-solutions. *Proceedings of 7th EUROCLAY Conference, Dresden, Germany*, pp. 441–446

Herrero, C.P. and Sanz, J. (1991) Short-range order of the Si,Al distribution in layer silicates. *Journal of the Physics and Chemistry of Solids*, **52**, 1129–1135.

Lear, P.R. and Stucki, J.W. (1990) Magnetic properties and site occupancy of iron in nontronite. *Clay Minerals*, **25**, 3–14.

Manceau, A., Lanson, B., Drits, V.A., Chateigner, D., Gates, W.P., Wu, J., Huo, D. and Stucki, J.W. (2000a) Oxidation-reduction mechanism of iron in dioctahedral smectites: I. Crystal chemistry of oxidized reference nontronites. *American Mineralogist*, **85**, 133–152.

Manceau, A., Drits, V., Lanson, B., Chateigner, D., Wu, J., Huo, D., Gates, W.P. and Stucki, J. (2000b) Oxidation-reduction mechanism of iron in dioctahedral smectites, II. Crystal chemistry of reduced Garfield nontronite. *American Mineralogist*, **85**, 153–172.

Palin, E.J., Dove, M.T., Redfern, S.A.T., Bosenick, A., Sainz-Díaz, C.I. and Warren, M.C. (2001) Computational study of tetrahedral Al-Si ordering in muscovite. *Physics and Chemistry of Minerals*, **28**, 534–544.

Palin, E.J., Dove, M.T., Redfern, S.A.T. and Sainz-Díaz, C.I. (2003) Computational study of tetrahedral Al-Si and octahedral Al-Mg ordering in phengite. *Physics and Chemistry of Minerals*, **30**, 293–304.

Palin, E.J., Dove, M.T., Hernández-Laguna, A. and Sainz-Díaz, C.I. (2004) A computational investigation of the Al/Fe/Mg order-disorder behavior in the dioctahedral sheet of phyllosilicates. *American Mineralogist*, **89**, 164–175.

Sainz-Díaz, C.I., Cuadros, J. and Hernández-Laguna, A. (2001a) Cation distribution in the octahedral sheet of dioctahedral 2:1 phyllosilicates by using inverse Monte Carlo methods. *Physics and Chemistry of Minerals*, **28**, 445–454.

Sainz-Díaz, C.I., Hernández-Laguna, A. and Dove, M.T. (2001b) Modelling of dioctahedral 2:1 phyllosilicates by means of transferable empirical potentials. *Physics and Chemistry of Minerals*, **28**, 130–141.

Sainz-Díaz, C.I., Palin, E.J., Hernández-Laguna, A. and Dove, M.T. (2003a) Octahedral cation ordering of illite and smectite. Theoretical exchange potential determination and Monte Carlo simulations. *Physics and Chemistry of Minerals*, **30**, 382–392.

Sainz-Díaz, C.I., Palin, E.J., Dove, M.T. and Hernández-Laguna, A. (2003b) Monte Carlo simulations of ordering of Al, Fe, and Mg cations in the octahedral sheet of smectites and illites. *American Mineralogist*, **88**, 1033–1045.

Schröder, K.-P., Sauer, J., Leslie, M., Catlow, C.R.A. and Thomas, J.M. (1992) Bridging hydroxyl groups in zeolitic catalysts: a computer simulation of their structure, vibrational properties and acidity in protonated faujasites (H-Y zeolites). *Chemical Physics Letters*, **188**, 320–325.

Schroeder, P.A. (1993) A chemical, XRD, and ^{27}Al MAS NMR investigation of Miocene Gulf Coast shales with application to understanding illite-smectite crystal-chemistry. *Clays and Clay Minerals*, **41**, 668–679.

Tsipursky, S.I. and Drits, V.A. (1984) The distribution of octahedral cations in the 2:1 layers of dioctahedral smectites studied by oblique-texture electron diffraction. *Clay Minerals*, **19**, 177–193.

Vantelon, D., Montarges-Pelletier, E., Michot, L.J., Briois, V., Pelletier, M. and Thomas, F. (2003) Iron distribution in the octahedral sheet of dioctahedral smectites. An Fe K-edge X-ray absorption spectroscopy study. *Physics and Chemistry of Minerals*, **30**, 44–53.

Warren, M.C., Dove, M.T., Myers, E.R., Bosenick, A., Palin, E.J., Sainz-Díaz, C.I., Guiton, B. and Redfern, S.A.T. (2001) Monte Carlo methods for the study of cation ordering in minerals. *Mineralogical Magazine*, **65**, 221–248.

Winkler, B., Dove, M.T. and Leslie, M. (1991) Static lattice energy minimization and lattice dynamics calculations on aluminosilicate minerals. *American Mineralogist*, **76**, 313–331.

Winkler, B., Pickard, C. and Milman, V. (2002) Applicability of a quantum mechanical 'virtual crystal approximation' to study Al/Si-disorder. *Chemical Physics Letters*, **362**, 266–270.

(*Received 20 August 2003; revised 22 December 2003; Ms. 828; A.E. Randall T. Cygan*)